Multi-level signaling in the Stokes space and its application to large-capacity optical communications

Kazuro Kikuchi[1,*] **and Shojiro Kawakami**[2]

[1]*Department of Electrical Engineering and Information Systems, the University of Tokyo 7-3-1 Hongo, Bunkyo-Ku, Tokyo 113-8656, Japan*
[2]*Photonic Lattice, Inc., ICR Building 2F, 6-6-3 Minami-Yoshinari, Aoba-Ku, Sendai, Miyagi 989-3204, Japan*

[*]*kikuchi@ginjo.t.u-tokyo.ac.jp*

Abstract: The Stokes vector of an optical signal does not depend on its absolute phase; therefore, we can construct the phase-insensitive optical communication system, using the Stokes vector as a modulation parameter. In such a system, multi-level optical signals can effectively be designed in the three-dimensional Stokes space and demodulated either by direct detection or by coherent detection, where low-complexity digital-signal processing (DSP) is employed. Although this system has the disadvantage that adaptive equalizers can hardly be implemented in the digital domain, it is still an attractive solution to large-capacity ($\geq$ 100 Gbit/s) and medium- or short-reach ($\leq$ 100 km) transmission. In this paper, we discuss the receiver configuration for the multi-level signal in the Stokes space and the efficient DSP algorithm for demodulating such a signal. Simulation results demonstrate that 2-, 4-, 8-, 16-, and 32-ary signals in the Stokes space have good bit-error rate (BER) characteristics. Especially, the 16-ary signal at the moderate symbol rate of 25 Gsymbol/s can reach the bit rate of 100 Gbit/s even by using direct detection.

OCIS codes: (060.2330) Fiber optics communications; (060.1660) Coherent communications; (060.4080) Modulation.

References and links

1. E. Yamazaki, S. Yamanaka, Y. Kisaka, T. Nakagawa, K. Murata, E. Yoshida, T. Sakano, M. Tomizawa, Y. Miyamoto, S. Matsuoka, J. Matsui, A. Shibayama, J. Abe, Y. Nakamura, H. Noguchi, K. Fukuchi, H. Onaka, K. Fukumitsu, K. Komaki, O. Takeuchi, Y. Sakamoto, H. Nakashima, T. Mizuochi, K. Kubo, Y. Miyata, H. Nishimoto, S. Hirano, and K. Onohara, "Fast optical channel recovery in field demonstration of 100-Gbit/s Ethernet over OTN using real-time DSP, " Opt. Express **19**, 13139-13184 (2011).
2. G. R. Welti and J. S. Lee, "Digital transmission with coherent four-dimensional modulation," IEEE Trans. on Information Theory **IT-20**, 497-502 (1974).
3. M. Karlsson and E. Agrell, "Which is the most power-efficient modulation format in optical links?," Opt. Express **17**, 10814-10819 (2009).
4. E. Agrell and M. Karlsson, "Power-efficient modulation formats in coherent transmission systems," J. of Lightwave Technol. **27**, 5115-5126 (2009).
5. K. Kikuchi, "Digital coherent optical communication systems: Fundamentals and future prospects," IEICE Electron. Express **8**, 1642-1662 (2011).
6. S. Benedetto and P. T. Poggiolini, "Multilevel polarization shift keying: Optimum receiver structure and performance evaluation," IEEE Trans. on Comm. **42**, 1174-1186 (1994).

#201666 - $15.00 USD Received 22 Nov 2013; revised 24 Jan 2014; accepted 4 Mar 2014; published 24 Mar 2014

7. S. Benedetto, A. Djupsjöbacka, B. Lagerström, R. Paoletti, P. Poggiolini, and G. Mijic, "Multilevel polarization modulation using a specifically designed $LiNbO_3$ device," IEEE Photon. Technol. Lett. **6**,949-951 (1994).
8. S. Benedetto, R. Gaudino, and P. Poggiolini, "Direct detection of optical digital transmission based on polarization shift keying modulation," IEEE J. Sel. Areas in Comm. **13**, 531-541 (1995).
9. S. Betti, F. Curti, G. De Marchis, and E. Iannone, "Multilevel coherent optical system based on Stokes parameters modulation," J. Lightwave Technol. **8**, 1127-1136 (1990).
10. S. Benedetto, R. Gaudino, and P. Poggiolini, "Polarization recovery in optical polarization shift-keying systems," IEEE Trans. on Comm. **45**, 1269-1279 (1997).
11. C. Brosseau, *Fundamentals of polarized light* (John Wiley & Sons, Inc. 1998).
12. K. Kikuchi and S. Tsukamoto, "Evaluation of sensitivity of the digital coherent receiver," J. of Lightwave Technol. **26**, 1817-1822 (2008).
13. S. J. Savory, "Digital filters for coherent optical receivers," Opt. Express **16**, 804-817 (2008).
14. Y. Mori, C. Zhang, and K. Kikuchi, "Novel configuration of finite-impulse-response filters tolerant to carrier-phase fluctuations in digital coherent optical receivers for higher-order quadrature amplitude modulation signals," Opt. Express **20**, 26236-26251 (2012).

1. Introduction

The complex amplitude of the optical electric field is represented by its in-phase (I) and quadrature (Q) components; thus, we have two degrees of freedom realizing quadrature amplitude modulation (QAM) of a single-polarization optical carrier. On the other hand, the optical electric field has two degrees of freedom of polarizations. Now, the following question arises: How can we utilize these four degrees of freedom for enhancing the performance of optical communication systems?

Figure 1 shows the genealogy of optical modulation formats studied so far. The dual-polarization (DP) 4-QAM (or quadrature phase-shift keying: QPSK) format has been commercialized at the single-carrier bit rate as high as 100 Gbit/s [1]. In such a scheme, IQ components of two polarizations are independently modulated in a binary manner. On the other hand, coherent four-dimensional modulation was investigated in [2], where constellation points were designed in the four-dimensional vector space. Applying such an idea to coherent optical communication systems, we can constitute the four-dimensional vector space composed of IQ vectors of two polarizations. Recently, the most power-efficient modulation format called the polarization-switched QPSK (PS-QPSK) format has been found out in the four-dimensional vector space [3, 4]. The receiver sensitivity of all of these modulation schemes depends on the carrier phase, and the newly-developed digital coherent receiver can demodulate them relying upon the digital phase-estimation technique [5].

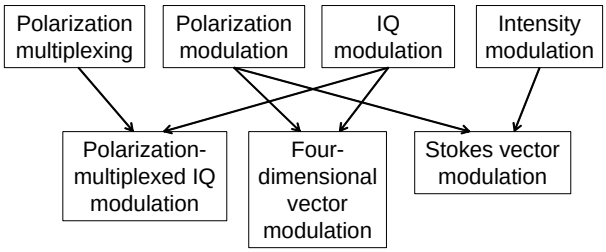

Fig. 1. Genealogy of optical modulation formats. IQ modulation and four-dimensional modulation are sensitive to the carrier phase. On the other hand, Stokes-vector modulation is independent of the absolute value of the carrier phase.

Meanwhile, optical communication systems based on multi-level modulation of the state of polarization (SOP) were studied a long time ago. The SOP including the intensity is expressed in terms of the Stokes vector $\mathbf{S} = [S_1, S_2, S_3]^T$, and we can effectively design the multi-level

#201666 - $15.00 USD Received 22 Nov 2013; revised 24 Jan 2014; accepted 4 Mar 2014; published 24 Mar 2014

signal in the three-dimensional Stokes space [6]. The signal modulated in the Stokes space is independent of the absolute phase of the carrier, but is dependent on the relative phase and the amplitude ratio between the *x*- and *y*-polarization component. Such Stokes-vector modulation is a natural extension of intensity modulation, which is immune to the carrier phase, adding two degrees of freedom of SOP to one-dimensional intensity modulation as shown in Fig. 1.

Multi-level SOP modulation was demonstrated by using a $LiNbO_3$ device [7]. In [8] and [9], direct detection and coherent detection of the Stokes vector were studied, respectively, and their bit-error rate (BER) performances were analyzed theoretically. In addition, the method for tracking SOP fluctuations during propagation through a fiber was discussed in [10].

Following such preceding researches, this paper puts Stokes-vector modulation in the spotlight again with the help of state-of-the-art digital signal-processing (DSP) technologies, which have been introduced in 100-Gbit/s digital coherent receivers. We develop an efficient DSP algorithm, which enables to track SOP fluctuations stemming from the random change in fiber birefringence and demodulate multi-level Stokes-vector modulation signals. Our simulation results show that the DSP circuit implemented in direct-detection receivers or coherent receivers can track such SOP fluctuations, using the decision-feedback control in a symbol-by-symbol manner, and that we can obtain high system performance and stability owing to the fast tracking speed of the DSP circuit. In addition, our DSP algorithm can cope with any Stokes-vector modulation format in a unified manner under severe conditions of carrier-phase fluctuations as well as SOP fluctuations. In fact, we demonstrate that 2-, 4-, 8-, 16-, and 32-ary signals in the Stokes space have good BER characteristics. The bit rate as high as 100 Gbit/s is obtained especially when we employ the 16-ary signal at the moderate symbol rate of 25 Gsymbol/s and the sampling rate of 25 GSa/s even in direct-detection systems. Although the Stokes-vector modulation system has the disadvantage that adaptive equalizers can hardly be implemented in the digital domain, it is a cost-effective solution to large-capacity ($\geq$ 100 Gbit/s) and medium- or short-reach ($\leq$ 100 km) transmission, where the time-varying effect from polarization-mode dispersion (PMD) is ignored.

This paper is organized as follows: Section 2 reviews the definition of Stokes vectors, the method of Stokes-vector modulation, and the method of Stokes-vector detection. In Sec. 3, we propose a direct-detection receiver and a coherent receiver, which can demodulate the multi-level signal in the Stokes space using low-complexity DSP. In Sec. 4, after analyzing noise characteristics of the Stokes vector, we perform intensive computer simulations on BERs of 2-, 4-, 8-, 16-, and 32-ary signals in the Stokes space. Section 5 concludes the paper.

2. Review on methods of Stokes-vector modulation and detection

2.1. Definition of Stokes vectors

Let E_x and E_y respectively be the *x*-polarization and *y*-polarization component of the complex amplitude of the signal electric field. The Jones vector of the signal is then expressed as

$$\mathbf{E} = \begin{bmatrix} E_x \\ E_y \end{bmatrix} \tag{1}$$

and transformed into the Stokes vector $\mathbf{S} = [S_1, S_2, S_3]^T$ [11] as

$$\begin{aligned} S_1 &= |E_x|^2 - |E_y|^2 , && (2)\\ S_2 &= 2\mathrm{Re}\left(E_x^* E_y\right) \\ &= 2|E_x||E_y|\cos\delta , && (3)\\ S_3 &= 2\mathrm{Im}\left(E_x^* E_y\right) \\ &= 2|E_x||E_y|\sin\delta , && (4) \end{aligned}$$

#201666 - $15.00 USD Received 22 Nov 2013; revised 24 Jan 2014; accepted 4 Mar 2014; published 24 Mar 2014

where δ is the phase difference between y and x polarizations defined as

$$\delta = \arg\left(E_y/E_x\right) . \tag{5}$$

The amplitude of the Stokes vector is equal to the signal intensity as shown by

$$\begin{aligned} S_0 &= \sqrt{S_1^2+S_2^2+S_3^2} \\ &= |E_x|^2 + \left|E_y\right|^2 . \end{aligned} \tag{6}$$

The Stokes vector can also be obtained from light intensities as follows: Let I_x be the light intensity of the x-polarization component of the signal, I_{45° that of the 45° linearly-polarized component with respect to the x axis, and I_R that of the right-circularly polarized component, respectively. The Stokes parameters S_1, S_2, and S_3 can be related to these intensities [11] as

$$S_1 = 2I_x - S_0 , \tag{7}$$

$$S_2 = 2I_{45^\circ} - S_0 , \tag{8}$$

$$S_3 = 2I_R - S_0 . \tag{9}$$

From Eqs. (2)-(4) as well as Eqs. (7)-(9), we find that the Stokes vector is obtained by square-law detection of signal complex amplitudes and does not include the absolute phase of the signal.

Stokes vectors are represented in the three-dimensional Stokes space. Especially when Stokes vectors are normalized such that $S_0 = 1$, they are distributed on the unit sphere called the Poincaré sphere, and each point on the sphere corresponds to SOP of the signal $\mathbf{E}$.

Using a signal amplitude A given as

$$A = \sqrt{|E_x|^2 + \left|E_y\right|^2} . \tag{10}$$

we can express Eq.(1) as

$$\mathbf{E} = Ae^{i\phi} \begin{bmatrix} \cos\left(\dfrac{\theta}{2}\right) \\ e^{i\delta}\sin\left(\dfrac{\theta}{2}\right) \end{bmatrix} . \tag{11}$$

In Eq. (11), ϕ is the absolute phase of the signal, and θ ($0 \le \theta \le \pi$) and δ ($-\pi/2 \le \delta \le \pi/2$) respectively determine the power ratio and the phase difference between y and x polarizations. Then, using Eqs. (2)-(4), we obtain the Stokes vector corresponding to Eq. (11) as

$$\mathbf{S} = S_0 \begin{bmatrix} \cos\theta \\ \sin\theta\cos\delta \\ \sin\theta\sin\delta \end{bmatrix} , \tag{12}$$

where $S_0 = A^2$. The Stokes vector $\mathbf{S}$ given by Eq. (12) is illustrated in Fig. 2.

Since the Stokes vector does not include the absolute phase of the carrier ϕ, the demodulation of Stokes-vector-modulated signals does not require the carrier estimation process similarly to the demodulation of intensity-modulated signals. On the other hand, the Stokes vector can be multi-level modulated in the three-dimensional Stokes space, whereas the intensity is modulated only one-dimensionally. This fact means that Stokes-vector modulation has much more freedom to design multi-level signals than intensity modulation in spite of its phase-insensitive nature.

#201666 - $15.00 USD Received 22 Nov 2013; revised 24 Jan 2014; accepted 4 Mar 2014; published 24 Mar 2014

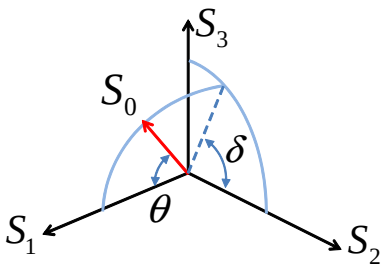

Fig. 2. Illustration of the signal SOP and the intensity in the Stokes space.

2.2. *Multi-level modulation of Stokes vectors*

In the Stokes-vector modulation scheme, a symbol mapper at the transmitter maps a symbol into a constellation point in the Stokes space shown by Fig. 2, using a prescribed mapping table. Then, the desired Stokes vector is generated through modulation of S_0, θ, and δ in Eq. (12).

Following Eq. (11), we can construct the Stokes-vector modulator shown in Fig. 3 [7]. The amplitude modulator (AM1) modulates the signal intensity S_0. The amplitude modulator (AM2) is a Mach-Zehnder modulator which splits the intensity-modulated signal into two output ports with an arbitrary splitting ratio by controlling θ. The phase modulator (PM) gives the phase difference δ between the split signals. The linear polarization of one of the paths is rotated by 90° by a half-wave plate ($\lambda/2$). These signals from the two paths have orthogonal linear polarizations and are combined with a polarization-beam combiner (PBC).

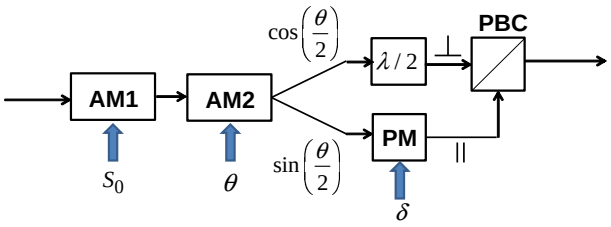

Fig. 3. Structure of the Stokes-vector modulator. AM: amplitude modulator, PM: phase modulator, $\lambda/2$: half-wave plate, and PBC: polarization-beam combiner. Symbols $\parallel$ and $\perp$ respectively show parallel and perpendicular linear polarizations.

For multi-level modulation of Stokes vectors, we should maximize the Euclidean distance between nearest constellation points in the Stokes space under the condition that S_0 is constant. Figure 4 shows constellation maps for binary, quad, and octal Stokes-vector modulation [8]. In the case of binary modulation, two constellation points are located at antipodal points. Constellation points in quad modulation are set at four vertices of a regular tetrahedron, whereas those in octal modulation at eight vertices of a regular hexahedron. Hereafter, we call the unit vector, which is directed from the origin to each constellation point in the Stokes space, *the basis Stokes vector*. In addition to such multi-level SOP modulation, multi-level modulation of S_0 can increase the number of modulation levels.

#201666 - $15.00 USD Received 22 Nov 2013; revised 24 Jan 2014; accepted 4 Mar 2014; published 24 Mar 2014

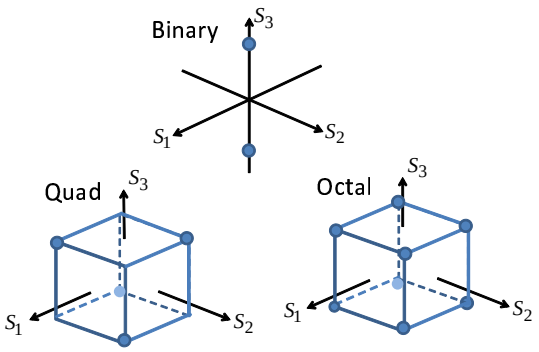

Fig. 4. Constellation maps in the Stokes space. We show those of binary, quad, and octal modulation. In addition, S_0 can be modulated at the same time.

2.3. *Detection of Stokes vectors*

Figure 5 shows the schematic diagram of the Stokes analyzer [8, 11], which can determine the Stokes vector based on direct detection. In the first branch, we measure the signal intensity S_0 with a photodiode (PD). Inserting a polarizer (0° Pol), whose transmission axis is the x axis, in the second branch, we measure the intensity I_x. Using a polarizer (45° Pol), whose transmission-axis is rotated by 45° with respect to the positive x axis, we detect the intensity I_{45° in the third branch. With a quarter-wave plane ($\lambda/4$), whose fast axis is aligned to the x axis, and a 45°-rotated polarizer (45° Pol), we measure the intensity I_R in the fourth branch. The Stokes vector is then calculated from Eqs. (6)-(9).

On the other hand, when we use a homodyne receiver comprising phase and polarization diversities [5], the Stokes vector is obtained from measured complex amplitudes E_x and E_y by using Eqs. (2)-(4).

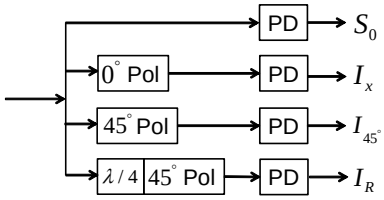

Fig. 5. Schematic diagram of the Stokes analyzer. From the four outputs from PDs, we can determine the Stokes vector using Eqs. (6)-(9).

3. Receivers for the demodulation of Stokes-vector-modulated signals

3.1. *Direct-detection receiver*

Figure 6 shows our proposed direct-detection-based receiver for the demodulation of Stokes-vector-modulated signals. The incoming signal is pre-amplified by an Erbium-doped fiber amplifier (EDFA). After passing through an optical compensator for group-velocity dispersion (GVD) of the fiber, the signal is filtered out to reduce amplified spontaneous emission (ASE) from the EDFA. Then, the signal is incident on the Stokes analyzer given in Fig. 5.

#201666 - $15.00 USD Received 22 Nov 2013; revised 24 Jan 2014; accepted 4 Mar 2014; published 24 Mar 2014

If the carrier-to-noise ratio (CNR) at the optical stage is determined from the average signal power and the associated shot noise, the reduction of the CNR in each branch is as low as $1/\mathrm{NF}$ owing to optical pre-amplification before the power splitter, where NF is the noise figure of the EDFA. Throughout this paper, however, we used the CNR value of the signal after detection; therefore, its value is degraded by $1/\mathrm{NF}$ from the optical CNR.

Four outputs from the Stokes analyzer are converted to digital data using four-channel analog-to-digital converters (ADCs). The clock extracted from the second branch controls sampling instances of the ADCs. The sampling rate is thus one sample per symbol. The ADC outputs are sent to the Stokes-vector calculator, where the Stokes vector is determined by Eqs. (2)-(4). Next, the output of the Stokes-vector calculator is sent to the following DSP circuit.

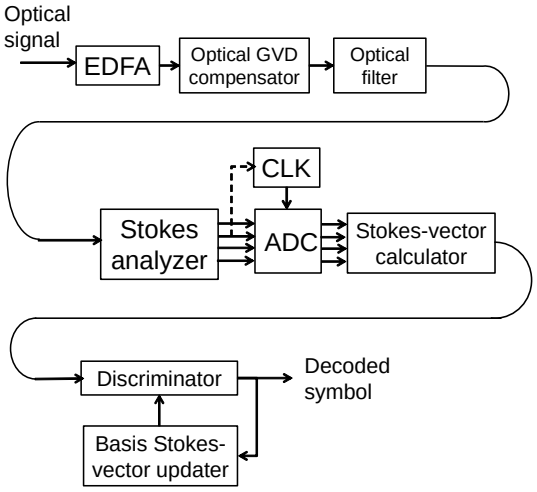

Fig. 6. Direct-detection-based receiver for the demodulation of Stokes-vector-modulated signals.

3.2. Coherent-detection receiver

Figure 7 shows the coherent-detection-based receiver for the demodulation of Stokes-vector-modulated signals. This coherent receiver is the homodyne receiver employing phase and polarization diversities. The optical CNR is degraded by 3 dB after detection [12]. If we introduce an optical pre-amplifier having the noise figure of NF before the coherent receiver, the total reduction of the CNR is $1/\mathrm{NF}$, which is the same as that in the direct-detection-based receiver [12]. Hereafter, we use the CNR after coherent detection for describing the signal quality.

Four outputs from the coherent receiver are converted to digital data using four-channel ADCs [5]. The clock for the ADCs can be extracted from the power of the *x*-polarization component, which is obtained from the analog output of the coherent receiver. After fixed equalization of accumulated GVD of the fiber and spectral filtering of the signal in the digital domain, the Stokes vector $\mathbf{S}$ is calculated from Eqs. (2)-(4) and sent to the following DSP circuit. Note that in contrast to the direct-detection-based receiver shown in Fig. 6, the coherent receiver enables fixed GVD compensation and signal filtering in the digital domain.

In principle, it is possible to introduce adaptive equalizers controlling the Jones vector into the DSP circuit; actually, we can achieve adaptive equalization using finite-impulse-response (FIR) filters in the butterfly-configuration adapted by the decision-directed least-mean-square (LMS) algorithm [13]. However, the decision-feedback process involved in such adaptive

#201666 - $15.00 USD Received 22 Nov 2013; revised 24 Jan 2014; accepted 4 Mar 2014; published 24 Mar 2014

equalization seriously suffers from carrier-phase fluctuations [14]. In such a case, computational complexity of the DSP circuit becomes larger to cope with this problem, and the advantage of the Stokes-vector-modulation scheme is greatly diminished.

Therefore, as far as we do not include adaptive equalizers in the receiver, the direct-detection-based receiver is more cost-effective than the coherent-detection-based receiver. The advantage of the coherent receiver is that fixed GVD compensation can be done in the digital domain; on the other hand, the direct-detection receiver is more suitable for short-distance applications and/or 1.3-μm transmission systems, where optical GVD compensation is not necessary.

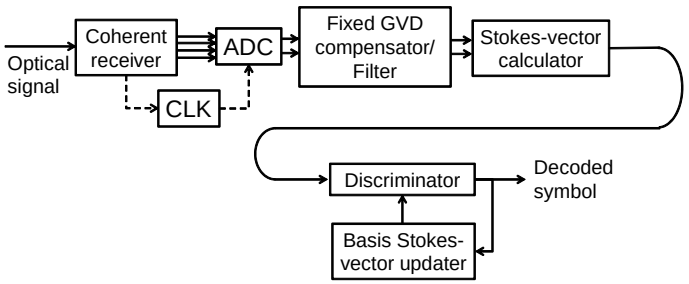

Fig. 7. Coherent-detection-based receiver for the demodulation of Stokes-vector-modulated signals.

3.3. DSP algorithm for symbol discrimination and polarization tracking

In both of the receivers described in 3.1 and 3.2, the calculated Stokes vector is processed by the same DSP algorithm as shown below.

We demodulate the signal by comparing the measured Stokes vector with basis Stokes vectors. In order to prepare the basis Stokes vectors at the receiver, the training sequence with a fixed SOP modulation pattern is transmitted through the fiber in advance. Assume that basis Stokes vectors thus obtained at the receiver are given as $\mathbf{v}_1(k)$, $\mathbf{v}_2(k)$, $\cdots$, $\mathbf{v}_n(k)$, where k denotes the number of samples and n the number of basis vectors. In binary, quad, and octal SOP modulations, n are 2, 4, and 8, respectively. Then, after taking the inner product between the received normalized Stokes vector $\mathbf{S}(k)/S_0$ and all of the n basis Stokes vectors, we find the basis vector $\mathbf{v}_m(k)$, which gives the maximum value of the inner products. The symbol is determined from the decided m-th basis Stokes vector, using the mapping table discussed in 2.2. When the intensity is simultaneously modulated, the measured S_0 is level-discriminated to find the symbol.

The basis Stokes vectors are fluctuating slowly due to the change in fiber birefringence, even if we have determined them using the training sequence; therefore, we need to track such fluctuations of the basis vectors. In the k-th sample, we have decided that the measured normalized Stokes vector is the m-th basis vector. Then, the m-th basis vector in the next symbol duration is updated by using the measured normalized Stokes vector as

$$\mathbf{v}_m(k+1) = \frac{\mathbf{v}_m(k) + \mu \mathbf{e}(k)}{\|\mathbf{v}_m(k) + \mu \mathbf{e}(k)\|} . \tag{13}$$

In Eq. (13), μ is a step-size parameter, and the error signal $\mathbf{e}(k)$ given as

$$\mathbf{e}(k) = \frac{\mathbf{S}(k)}{S_0(k)} - \mathbf{v}_m(k) \tag{14}$$

#201666 - $15.00 USD Received 22 Nov 2013; revised 24 Jan 2014; accepted 4 Mar 2014; published 24 Mar 2014

attempts to eliminate the deviation of the basis Stokes vector from its correct position. A smaller value of μ improves the signal-to-noise ratio of $\mathbf{v}_m(k)$ but reduces the SOP tracking speed; therefore, we need to choose an optimum value of μ, depending on the SOP fluctuation speed.

It should be noted that we do not update the *m*-the basis Stokes vector and keep its value until the next symbol where the *m*-the basis Stokes vector is selected again. However, since the speed of SOP fluctuations is much slower than the symbol rate, such thinned-out operation of the update process never degrades the BER performance. In addition, the decision-feedback process included in Eq. (13) does not have any serious problem for circuit implementation owing to the slow SOP fluctuation speed.

Compared with the digital coherent receiver for the DP-QPSK signal, Fig. 7 has much simpler structure, because DSP circuits for carrier phase estimation and adaptive equalization are not included. On the other hand, since adaptive equalization cannot be implemented in our receiver, the Stokes-vector modulation format may be mainly applied to transmission systems shorter than 100 km, where PMD is not significant.

4. Receiver-sensitivity analyses of the Stokes-vector modulation scheme

4.1. Noise distribution in the Stokes space

The Stokes vector is obtained by square-law detection of the complex amplitude of the optical electric field. Therefore, the noise distribution of the Stokes vector is broader than that of the complex amplitude, which results in the degradation of the BER performance of the Stokes-vector modulation scheme compared with the IQ modulation scheme. In 4.1, we compare the noise distribution of the Stokes vector with that of the IQ vector through numerical calculations in order to have comprehensive understanding of the BER performance in 4.2.

Adding white Gaussian noise to a unity signal amplitude with *x* polarization, we define the Jones vector as

$$\mathbf{E} = \begin{bmatrix} 1+n_x \\ n_y \end{bmatrix} . \tag{15}$$

In Eq. (15), n_x and n_y are complex-valued Gaussian noises with *x* and *y* polarizations, respectively. The variance of the real part and that of the imaginary part of these noises are given as σ^2. Since CNR per polarization (CNR/pol) means the ratio between the average signal power and the power of the single-polarization noise, it is given as

$$\text{CNR/pol} = \frac{1}{2\sigma^2} . \tag{16}$$

Figure 8 shows probability-density functions for the in-phase and quadrature components of the complex amplitude of the signal. Blue curves are simulation results, whereas red ones are Gaussian fits to them, when CNR/pol=7, 10, and 15 dB.

Next, we transform the Jones vector given by Eq. (15) into the Stokes vector, using Eqs. (2)-(4), and calculate probability-density functions for Stokes parameters S_1, S_2, and S_3, when CNR/pol=7, 10, and 15 dB. Blue curves are simulation results, whereas red ones are Gaussian fits to them. These probability-density functions differ from Gaussian distributions and such difference is remarkable when CNR/pol becomes lower. As shown by Figs. 8 and 9, probability-density functions of the Stokes parameters are much broader than those of the IQ components when CNR/pol is the same. This means that the receiver sensitivity in the Stokes-vector modulation scheme is generally lower than that in the IQ-modulation scheme. In addition, we find that the probability-density function of the Stokes vector has a steeper slope when the S_1 value decreases along the radial direction of the Stokes vector. This fact implies that the receiver sensitivity in the Stokes-vector modulation scheme is dependent not only on the distance between nearest constellation points but also on the configuration of constellation points.

#201666 - $15.00 USD Received 22 Nov 2013; revised 24 Jan 2014; accepted 4 Mar 2014; published 24 Mar 2014

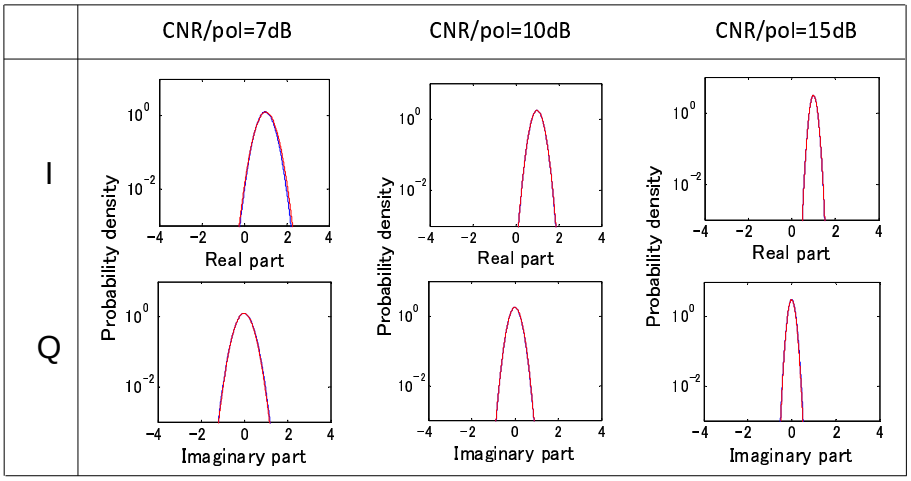

Fig. 8. Probability-density functions for the in-phase and quadrature components of the complex amplitude of the signal. Blue curves are simulation results, and red ones are Gaussian fits to them. Upper figures correspond to the in-phase component, whereas the lower figures to the quadrature component. Values of CNR/pol are 7, 10, and 15 dB.

In fact, Fig. 10 shows the comparison of probability-density functions of Stokes vectors among binary (black curve), quad (blue curve), and octal (red curve) modulation formats. In all of the modulation formats, we assume that CNR/bit/pol is 13 dB and the noise-free amplitude of the signal is unity. Note that CNR/pol defined in 4.1 is divided by the number of bits per symbol to evaluate the receiver sensitivity. We calculate probability-density functions along the line connecting two nearest constellation points, when the modulated SOP is in the positive side of the line. The origin of the distance is the center of the segment of the line. The symbol error occurs when the Stokes vector is distributed in the negative distance region. The binary and quad formats have almost the same distribution where the slope is positive, indicating that both formats have the very similar BER characteristics. On the other hand, the probability density of the octal format is higher than those of the binary and quad formats, when the distance is negative; hence, we can predict that the BER performance of the octal format is worse than those of the binary and quad formats.

4.2. BER characteristics

Through computer simulations, we calculate BER characteristics of the binary, quad, and octal SOP-modulation schemes as a function of the CNR/bit/pol. We also analyze 16-ary and 32-ary Stokes-vector modulation schemes, where the intensity in the octal SOP-modulation scheme is modulated in 2-level and 4-level manners, respectively. In the 16-ary modulation scheme, the intensity S_0 is modulated between I_0 and $3I_0$, and the threshold of the level discrimination is set at $2I_0$ to obtain the best BER performance. In the 32-ary modulation scheme, on the other hand, the intensity modulation is performed among four levels, I_0, $2I_0$, $4I_0$, and $6I_0$. Thresholds for the level discrimination are $1.5I_0$, $3I_0$, and $5I_0$. Those parameters are determined so that the best BER performance is obtained. In these modulation schemes accompanying the intensity modulation, we define CNR using the average signal power. Note that since we define CNR/bit/pol after detection, BER characteristics are not dependent on the choice of receivers between Fig. 6 and Fig. 7.

#201666 - $15.00 USD Received 22 Nov 2013; revised 24 Jan 2014; accepted 4 Mar 2014; published 24 Mar 2014

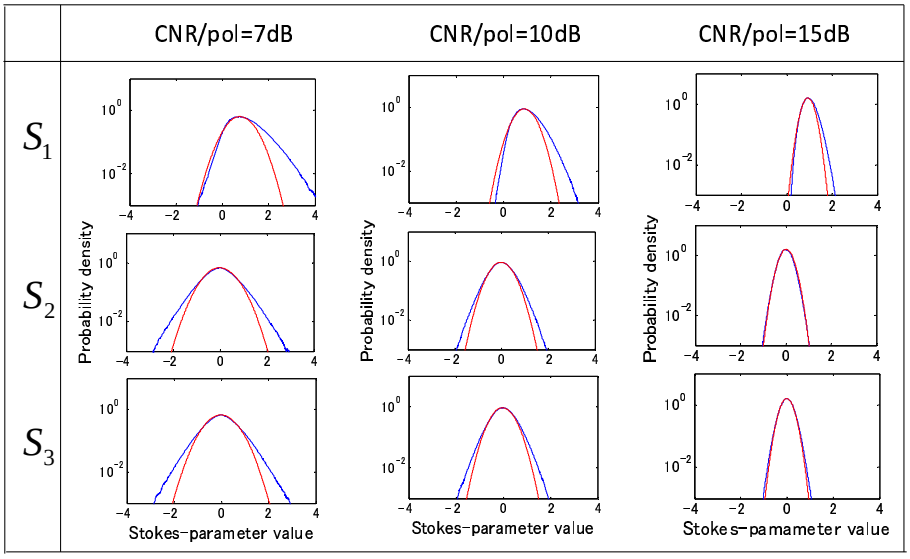

Fig. 9. Probability-density functions of Stokes parameters. Blue curves are simulation results for S_1, S_2, and S_3, whereas red ones are Gaussian fits to them. Values of CNR/pol are 7, 10, and 15 dB.

In the simulations, we first prepare the sequence of the Jones vector having a certain value of CNR/bit/pol and the number of symbols $N = 2^{20}$. The value of CNR/bit/pol is controlled by the amount of Gaussian noise. We also assume that $\delta f \cdot T = 10^{-2}$. The parameter δf denotes the linewidth of the transmitter laser in the direct-detection case, whereas it denotes the sum of linewidths of the transmitter laser and the local oscillator in the coherent-detection case. The parameter T is the symbol duration. Supposing that the symbol rate is 10 Gsymbol/s, the linewidth of the laser in the direct-detection system is as wide as 100 MHz, and that in the coherent system is 50 MHz. Those values are much larger than the linewidth of common distributed feedback (DFB) semiconductor lasers.

Next, we scramble the SOP of the signal to emulate the random fluctuation of fiber birefringence. Let the fiber birefringence be expressed by the Jones matrix as

$$\mathbf{J} = \begin{bmatrix} e^{i\frac{\phi_r}{2}} \cos\left(\frac{\theta_r}{2}\right) & -\sin\left(\frac{\theta_r}{2}\right) \\ \sin\left(\frac{\theta_r}{2}\right) & e^{-i\frac{\phi_r}{2}} \cos\left(\frac{\theta_r}{2}\right) \end{bmatrix} . \tag{17}$$

The polar angle and the azimuthal angle of SOP randomly fluctuate on the Poincaré sphere in a symbol-by-symbol manner through ϕ_r and θ_r. Parameters ϕ_r and θ_r obey the following equations:

$$\phi_r(k+1) = \phi_r(k) + \Delta\phi_r(k) , \tag{18}$$
$$\theta_r(k+1) = \theta_r(k) + \Delta\theta_r(k) , \tag{19}$$

where k is the number of symbols, and $\Delta\phi_r(k)$ and $\Delta\theta_r(k)$ are real-valued Gaussian noises. In our simulations, we assume that their standard deviations are commonly given as $\sqrt{\sigma_0^2} = 2 \times 10^{-3}$ [rad]. Since $\phi_r(k)$ and $\theta_r(k)$ are random-walk parameters, their variance $\sigma(N)^2$ at the

#201666 - $15.00 USD Received 22 Nov 2013; revised 24 Jan 2014; accepted 4 Mar 2014; published 24 Mar 2014

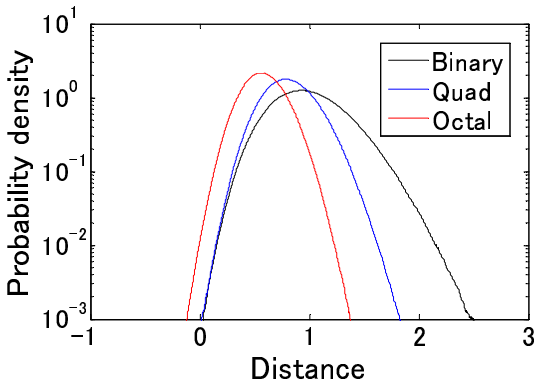

Fig. 10. Probability-density functions for Stokes vectors in binary (black curve), quad (blue curve), and octal (red curve) SOP modulation formats along the line connecting two nearest constellation points in each modulation format. The horizontal axis represents the distance along the line where the origin is the center of the segment of the line. The signal amplitude is unity, and CNR/bit/pol is 13 dB in all of the cases.

N-th symbol is written as

$$\sigma(N)^2 = \sigma_0^2 N \quad [\mathrm{rad}^2]\,. \tag{20}$$

Since $N = 2^{20}$, $\sqrt{\sigma(N)^2} \simeq 2$ [rad]. In the 10-Gsymbol/s system, the total time span for 2^{20} symbols is about 100 μs, and the standard deviation of 2 rad in 100 μs is much larger than SOP fluctuations in real systems. Figure 11 shows symbol-by-symbol plots of SOP on the Poincaré sphere for 2^{20} symbols, when the Jones matrix given by Eq. (17) is operated to the initial Jones vector $\mathbf{E} = [1,0]^T$. We find that SOP randomly fluctuates on the Poincaré sphere starting from $\mathbf{S} = [1,0,0]^T$.

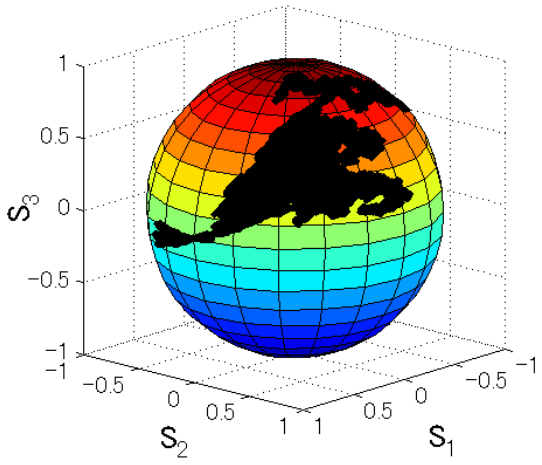

Fig. 11. Fluctuations of SOP due to the change in fiber birefringence. SOP is plotted in a symbol-by-symbol manner for $N = 2^{20}$ symbols, when the initial Jones vector is $\mathbf{E} = [1,0]^T$ and $\sqrt{\sigma_0^2} = 2 \times 10^{-3}$ [rad].

#201666 - $15.00 USD Received 22 Nov 2013; revised 24 Jan 2014; accepted 4 Mar 2014; published 24 Mar 2014

Finally, the Jones vector including SOP fluctuations is converted to the Stokes vector. The Stokes vector is demodulated by the algorithm given in 3.3, where the step-size parameter μ is $1/2^7$. Then, the number of bit errors is counted.

Figure 12 shows BERs for binary, quad, octal, 16-ary, and 32-ary modulation formats calculated as a function of CNR/bit/pol. We have confirmed that these curves are influenced neither by laser linewidths nor by SOP fluctuations. For comparison, the BER curve for the DP-QPSK format is also shown in Fig. 12, where laser linewidths and SOP fluctuations are neglected.

We find that the binary and quad formats have almost the same BER characteristics. On the other hand, the receiver sensitivity of the octal format is worth than those of the binary and quad formats by 2 dB at BER=10^{-5}. These results are in good agreement with the prediction from probability-density functions of Stokes vectors, which was discussed in 4.1.

The 16-ary modulation format can reach 100 Gbit/s at the moderate symbol rate of 25 Gsymbol/s and the ADC sampling rate of 25 GSa/s even in direct-detection systems. The sensitivity degradation from the binary modulation scheme is 3 dB, and that from the DP-QPSK format is 7 dB at BER=10^{-5}. This format seems very attractive for medium- or short-reach ($\leq$ 100 km) 100-Gbit/s transmission because of its low computational complexity of DSP, although the receiver sensitivity is lower than the DP-QPSK format and adaptive equalization is difficult to achieve.

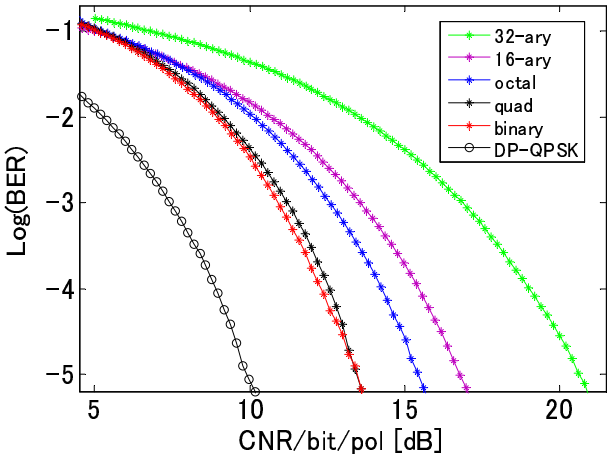

Fig. 12. BERs for binary, quad, octal, 16-ary, and 32-ary modulation formats calculated as a function of CNR/bit/pol. The BER curve for the DP-QPSK format is also shown for comparison.

5. Conclusions

In this paper, we have discussed the receiver configuration for the multi-level signal in the Stokes space and the efficient DSP algorithm for demodulating such a signal. Either direct-detection receivers or coherent receivers can demodulate such a multi-level signal using low-complexity DSP. Intensive computer simulations show that 2-, 4-, 8-, 16-, and 32-ary signals in the Stokes space have good bit-error rate (BER) characteristics. The bit rate as high as 100 Gbit/s is obtained especially when we employ the 16-ary signal in the Stokes space at the moderate symbol rate of 25 Gsymbol/s and ADC sampling rate of 25 GSa/s. Although the Stokes-vector modulation system has the disadvantage that adaptive equalizers cannot be implemented in the digital domain and its receiver sensitivity is lower than that of the IQ modulation sys-

#201666 - $15.00 USD Received 22 Nov 2013; revised 24 Jan 2014; accepted 4 Mar 2014; published 24 Mar 2014

tem, it is a cost-effective solution to large-capacity ($\geq$ 100 Gbit/s) and medium- or short-reach ($\leq$ 100 km) transmission.

Acknowledgments

This work was supported in part by Grant-in-Aid for Scientific Research (A) (25249038), the Ministry of Education, Culture, Sports, Science and Technology in Japan.

#201666 - $15.00 USD Received 22 Nov 2013; revised 24 Jan 2014; accepted 4 Mar 2014; published 24 Mar 2014